ACSNANO
www.acsnano.org
ARTICLE

Modulation of Quantum Tunneling *via* a Vertical Two-Dimensional Black Phosphorus and Molybdenum Disulfide p–n Junction

Xiaochi Liu,[†,#] Deshun Qu,[†,#] Hua-Min Li,[‡] Inyong Moon,[†] Faisal Ahmed,[§] Changsik Kim,[†] Myeongjin Lee,[†] Yongsuk Choi,[†] Jeong Ho Cho,[†,∥] James C. Hone,[⊥] and Won Jong Yoo*[,†,§]

[†]Department of Nano Science and Technology, SKKU Advanced Institute of Nano-Technology (SAINT), [§]School of Mechanical Engineering, and [∥]School of Chemical Engineering, Sungkyunkwan University, Suwon 16419, Republic of Korea

[‡]Department of Electrical Engineering, University at Buffalo, The State University of New York, Buffalo, New York 14260, United States

[⊥]Department of Mechanical Engineering, Columbia University, New York, New York 10027, United States

S *Supporting Information*

ABSTRACT: **Diverse diode characteristics were observed in two-dimensional (2D) black phosphorus (BP) and molybdenum disulfide (MoS_2) heterojunctions. The characteristics of a backward rectifying diode, a Zener diode, and a forward rectifying diode were obtained from the heterojunction through thickness modulation of the BP flake or back gate modulation. Moreover, a tunnel diode with a precursor to negative differential resistance can be realized by applying dual gating with a solid polymer electrolyte layer as a top gate dielectric material. Interestingly, a steep subthreshold swing of 55 mV/dec was achieved in a top-gated 2D BP–MoS_2 junction. Our simple device architecture and chemical doping-free processing guaranteed the device quality. This work helps us understand the fundamentals of tunneling in 2D semiconductor heterostructures and shows great potential in future applications in integrated low-power circuits.**

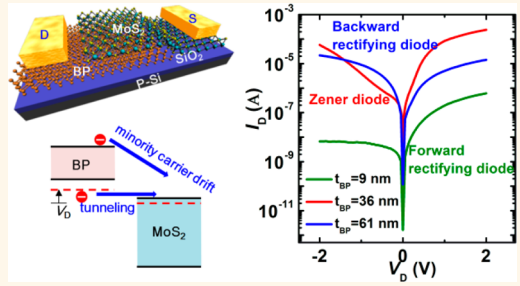

KEYWORDS: *2D heterojunction, diverse functional diode, tunneling transistor, black phosphorus, molybdenum disulfide*

Conventional metal–oxide–semiconductor field effect transistors (MOSFETs) using silicon are about to reach a fundamental scaling limit because of the short channel effects induced by degradations in electrostatic control. The fundamental thermionic limitation of the subthreshold swing (SS) is another challenge to MOSFETs.[1] Tunnel field effect transistors (TFETs) are considered to be a leading solution for achieving a subthermionic SS of <60 mV/dec *via* quantum mechanical band-to-band tunneling (BTBT), which will decrease the power consumption.[2−4] Two-dimensional (2D) semiconducting materials[5−8] are promising for TFET applications since they possess energy band gaps in a range of 0.4−1.2 eV, which is appropriate for scaled, low-power devices. Their ultrathin bodies make a smaller tunneling distance possible, giving rise to a high tunneling current. The absence of dangling bonds on the surface of 2D semiconductors provides sharp band edges with minimal trap states.[9,10] The realization of TFETs requires highly staggered or broken-gap band alignments, in which highly doped semiconductors[11] or thin-body semiconductors that can be easily modulated by electrostatic gating are usually used.[12]

Black phosphorus (BP) is a promising 2D semiconducting material for use in TFETs since multilayer BP possesses a small direct band gap of ∼0.4 eV, a small transport effective mass (m^*) of 0.15m_0, an anisotropic m^* that increases the density of states near the band edges, and a high mobility. A steep and clean junction can be formed between p- and n-type BP with the help of doping or electrostatic gating, potentially enabling a TFET with a subthermionic SS.[13] Unfortunately, BP is a temperamental p-type semiconductor that shows a strong pinning effect at the metal–BP interface.[14−16] Although aluminum (Al) contacts resulted in an n-type BP transistor,[17] it is still difficult to obtain homogeneous BP TFETs due to the limited gate tunability of this n-type BP transistor. Researchers are still seeking stable and effective doping methods for BP.[18,19]

Small band gap 2D transition metal dichalcogenides (TMDCs) with ambipolar performance, such as molybdenum ditelluride ($MoTe_2$) or tungsten diselenide (WSe_2), may be the

Received: June 8, 2017
Accepted: August 8, 2017
Published: August 8, 2017

DOI: 10.1021/acsnano.7b03994
ACS Nano XXXX, XXX, XXX–XXX

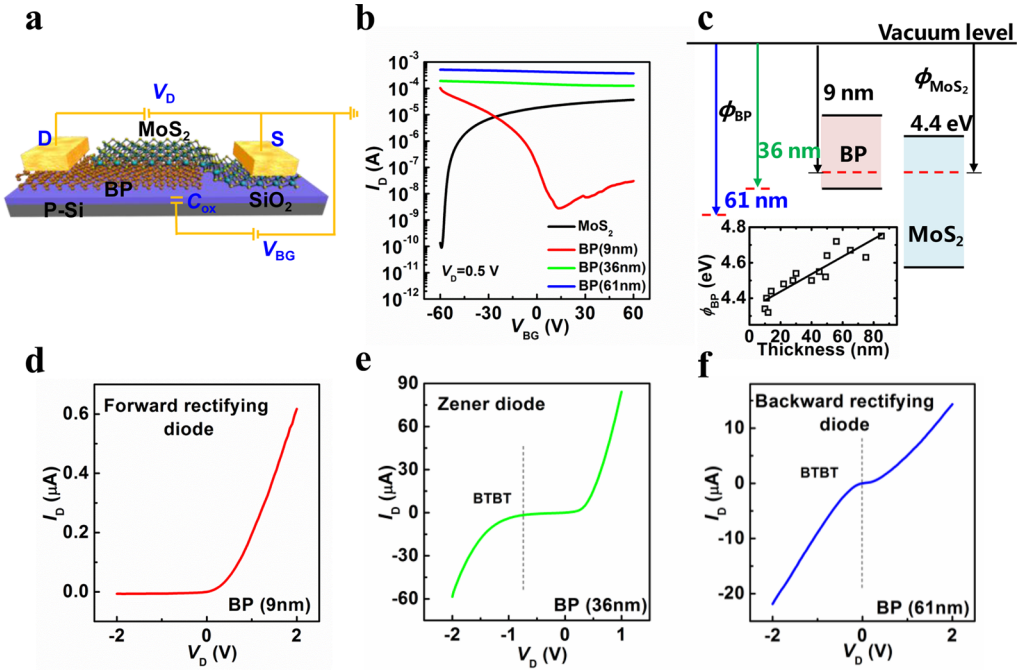

Figure 1. Device schematic and electrical performance characterization. (a) Schematic of BP−MoS_2 heterojunction device and the external circuit. (b) Transfer characteristics of MoS_2 and BP; BP flakes are of different thicknesses. (c) Band alignment between MoS_2 and BP. Work functions were obtained by KPFM; BP flakes of different thicknesses were measured. (d−f) Diverse diode properties of BP−MoS_2 heterojunctions composed of BP with different thicknesses.

next candidates.[20,21] However, reliable doping techniques for TMDCs have not been well developed so far.[22] The use of electrostatic gating techniques to realize a TFET requires dual gating, which adds design complexity and is not energy efficient.[23] Furthermore, the deposition of a high-quality high-*k* dielectric for effective gating of a TFET remains a challenge that must be addressed for TMDCs. Lateral WSe_2 TFETs have been achieved with the utilization of poly(ethylene oxide) and cesium perchlorate (PEO:$CsClO_4$) ion doping and top gating with a high-*k* Al_2O_3 dielectric[24] (where a large SS of 200 mV was achieved). 2D heterostructures with two different semiconductors stacked together could be a good approach to realize TFETs. One advantage of heterojunctions is that we have a big family of 2D materials with various carrier densities and electron affinities for the design of band alignments that can match the requirement of TFETs.[25] Second, vertical heterojunctions are more process-friendly compared to lateral homogeneous TFETs, which require precise patterning of the n- and p-type semiconductors.[26,27] Moreover, the vertical structure can provide a much larger planar junction area, which will give rise to a higher tunneling current. BP is a good option due to its small electron affinity and degenerate p-type properties with a certain thickness, as demonstrated in the BP−$SnSe_2$ Esaki diode.[28] Molybdenum disulfide (MoS_2) is naturally n-type, and the conduction band aligns with the band gap of BP. As such, MoS_2 could be another component used in a TFET with p-type BP.

BP−MoS_2 heterostructures have been fabricated to explore their photoelectric properties in several works.[29−31] However, we discovered the tunneling properties of this heterojunction. We found that the junction properties strongly depend on the BP thickness, while BP thickness actually modulates the doping level of the BP flakes. As the BP thickness increases, the BP−MoS_2 heterojunction can be tuned from a conventional forward rectifying p−n diode to a Zener diode and finally to a backward rectifying diode due to the activation of BTBT in thicker BP−MoS_2 heterojunctions. The transition between these diverse functional diodes can also be achieved through back gate modulation. A real tunnel diode formed between BP, MoS_2, and a precursor toward negative differential resistance (NDR)[28] was observed under a forward bias on BP by applying dual gating with a solid polymer electrolyte layer (PEO:$CsClO_4$) as a top gate dielectric material. The tunnel diode was transformed from the off-state to the on-state under top gate modulation with a small SS of 55 mV/dec. This work achieved a subthermionic SS with 2D semiconductors. Although thick BP (up to 72 nm) was used, the high doping concentration of thick BP flakes is what really matters for the realization of BP−MoS_2 TFETs. This mechanism is also applicable to atomically thin BP−MoS_2 heterojunctions once an appropriate doping method is developed for BP.

RESULTS AND DISCUSSION

Figure 1a shows schematics of the fabricated BP−MoS_2 heterojunction and the external device circuit. The device fabrication process is described in detail in the Methods section. We prepared several BP−MoS_2 heterojunction devices with various BP thicknesses. Optical microscopy images of the devices are shown in Supporting Information Figure S1 together with the flake thicknesses measured by atomic force microscopy (AFM). BP flakes were 9, 36, and 61 nm, whereas the thicknesses of the MoS_2 flakes were controlled in a small range of 6−12 nm. We deposited a pair of electrodes onto both BP and MoS_2 flakes to collect their electrical performances separately. For the junction, drain bias (V_D) is always applied to BP, while MoS_2 is the grounded source terminal. We plotted the transfer characteristics of BP with different thicknesses in Figure 1b. The transfer characteristics of MoS_2 flakes did not change much in the thickness range of 6−12 nm. A typical

DOI: 10.1021/acsnano.7b03994
ACS Nano XXXX, XXX, XXX−XXX

transfer curve of MoS_2 in this thickness range is shown by the black line in Figure 1b, displaying a normal n-type property with an on−off ratio of more than 10^5. The BP transistor fabricated from a 9 nm flake shows ambipolar transfer characteristics (red curve) with a much more pronounced hole branch than an electron branch. The on−off ratio of the hole branch reached almost 10^5, demonstrating a non-degenerate doping level for a 9 nm BP flake. As we mentioned above, the BP of a certain thickness becomes a degenerate p-type semiconductor; that is, the Fermi level of thick BP flake lies in the valence band. The negligible gate dependence observed from the transfer characteristics of BP transistors prepared by using 36 nm (green curve) and 61 nm (blue curve) thick BP may indicate their degeneracy. We also understand that a negligible gate dependence may result from the screening mechanism in thick flakes, which is related to the gating and contact geometries.[27] Nevertheless, the big difference in current level for thin and thick BP flakes at V_{BG} = 0 V is a discrepancy in doping levels since the band gap remains similar for BP flakes thicker than 5 layers. So, we measured the work functions (Φ) of fresh BP flakes with different thicknesses by Kelvin probe force microscopy (KPFM). BP flakes were rinsed with isopropyl alcohol (IPA) prior to KPFM measurement to remove the unintentional surface contaminations. The results are shown in Figure 1c. We did not measure the work function of the same BP flake used in the heterojunction device because BP is easily oxidized when it is exposed to air. We stacked MoS_2 onto the fresh BP surface inside a glovebox to ensure a good-quality BP−MoS_2 interface for better performance of the device. After completing the entire device processing, KPFM measurements on BP flakes did not show the real surface potential of the fresh BP flake. The work function of BP tends to increase with the flake thickness. Band alignment between BP and MoS_2 was established based on their work functions. The Fermi level of thin BP flakes is within the band gap and close to the valence band maximum (VBM), while that of thick BP flakes is located far below the VBM, which makes the thick BP flakes degenerate p-type, as we expected.

We then characterized the electrical properties of BP−MoS_2 heterojunction devices with various BP thicknesses. The device composed of 9 nm BP shows normal forward rectifying characteristics (Figure 1d) as observed from BP−MoS_2 p−n junctions reported previously.[29−31] That is, current under a forward V_D is much higher than that under a reverse V_D. When the BP thickness increased to 36 nm, the forward current showed a similar trend to the thin BP−MoS_2 device. The current started to increase when V_D was applied. Meanwhile, the reverse current stayed constant at a small V_D and started to increase dramatically at a critical reverse voltage of about −0.8 V (Figure 1e), which matches the performance of a Zener diode.[32] Generally, if a breakdown voltage is $<4E_g/q$, the breakdown can be assigned to Zener tunneling. Here, E_g is the band gap of the semiconductor, and q is the charge of an electron. Considering the smaller band gap of BP (E_g = 0.4 eV), the value of $4E_g/q$ is 1.6 V. Therefore, such a room-temperature reverse breakdown can be attributed to Zener breakdown originating from BTBT. When we further increased the BP thickness to 61 nm, the junction had a better conduction for reverse bias than for forward bias (Figure 1f), showing backward rectifying characteristics. The superior conduction in the reverse direction can also be attributed to BTBT, as will be explained below. In general, the BP−MoS_2 junction can be modulated between a forward rectifying diode, a Zener diode, and a backward rectifying diode by varying the BP thickness. Discrepancies in current conduction under reverse biases between those different functional diodes can also be easily discriminated by their output curves shown in a logarithmic scale (see Supporting Information Figure S2). In a forward rectifying diode configuration, the reverse current remains constant at a negative V_D as high as 4 V, and the forward to reverse rectification ratio ($I_{2\ V}/I_{-2\ V}$) approached 100. In contrast, the reverse current for the Zener diode and backward rectifying diode increased with a negative V_D. Contact issues can be excluded as an explanation for the different junction properties. Both BP and MoS_2 show quite linear and symmetric output curves at V_{BG} = 0 V (see Supporting Information Figure S3), and this demonstrates that the contact resistance was not important in the carrier transport through those hetero-junctions.[27] The realizations of a Zener diode and a backward rectifying diode were considered to be preliminary steps toward the eventual fabrication of TFETs. We are able to figure out the doping state of each component forming the diode by analyzing the diode properties, and we therefore changed the diode to make it an appropriate functional tunnel diode for the realization of TFETs. The special characteristics of backward rectifying diodes and Zener diodes make them suitable for a number of applications where other diodes may not perform as well. For example, backward rectifying diodes can be used as detectors for small signals since the current starts to flow under small reverse biases, while Zener diodes are commonly used in analog circuits.

The corresponding band diagrams for each diode were constructed as shown in Figure 2a, b, and c. Carrier transport in the forward direction for all these diodes followed the same mechanism as in a conventional p−n junction. Generally, the behavior can be described by the equation

$$I_{D(forward)} = I_S(e^{V_D/nV_T} - 1)$$

Here, I_D is the diode current, I_S is the reverse bias saturation current, V_D is the voltage across the diode, n is the ideality

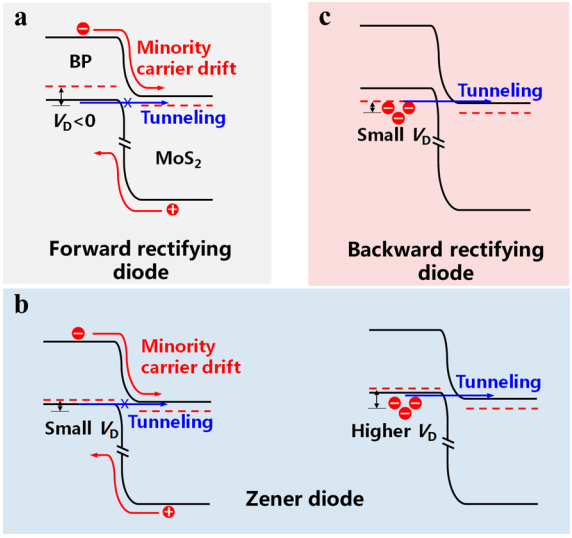

Figure 2. Band diagrams for BP−MoS_2 diodes of diverse functions. (a−c) Band diagrams corresponding to the forward rectifying diode, Zener diode, and backward rectifying diode, respectively. V_D on BP is negative, and carrier transport in the reverse direction of BP−MoS_2 diodes was studied.

DOI: 10.1021/acsnano.7b03994
ACS Nano XXXX, XXX, XXX−XXX

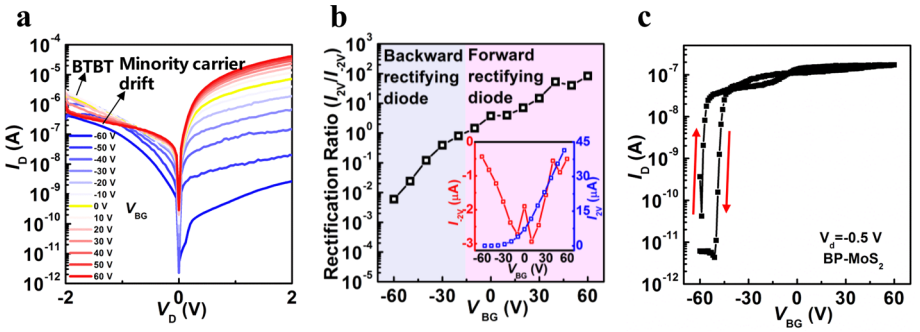

Figure 3. Gate-dependent diode properties. (a) Output curves of a BP−MoS_2 heterojunction device under various gate biases. (b) Plot of the device rectification ratio with respect to gate voltage. The forward and reverse current variation trend under back gate modulation is shown in the inset. (c) Transfer curves of a BP−MoS_2 junction. Both forward and reverse sweeps are shown.

factor, and V_T is the thermal voltage.[33] Ideally, the forward current would increase exponentially with V_D. This is actually a thermionic emission process. A forward V_D shifts down the band of BP to lower the interface barrier height. Hence, electrons in the conduction band of MoS_2 and holes in the valence band of BP can overcome the interface barrier and emit to their counterparts. Thus, forward conduction takes place. In contrast, the negative V_D shifts the BP band up and exaggerates the interlayer barrier. For a less doped thin BP flake, the Fermi level lies above the VBM, as we confirmed using KPFM. Band alignment between BP and MoS_2 under a reverse V_D is shown in Figure 2a. The reverse conduction is dominated by minority carrier drift. Electrons in the BP conduction band and holes in the MoS_2 valence band are the minority carriers. So, the reverse current is limited, since BP and MoS_2 are strong p- and n-type semiconductors, respectively. Therefore, the concentration of those minority carriers is intrinsically low. Because the VBM of BP aligns with the band gap of MoS_2, electron tunneling is also blocked, as shown by the blue arrow. In general, the device has better conduction in the forward direction than in the reverse direction as we observed from the forward rectifying diode in Figure 1c.

We confirmed by KPFM measurements that the work function of BP increased with the flake thickness. We expected that the Fermi level of 36 nm thick BP would be located at the VBM edge, as shown in Figure 2b. Under a small reverse V_D, the VBM of BP still aligned to the band gap of MoS_2, as shown in the left panel of Figure 2b. In this case, carrier transport is dominated by the minority carrier drift as we described above for the forward rectifying diode. So, the drain current displayed a plateau under a small negative V_D modulation as observed from the reverse current of a forward rectifying diode. When a higher reverse V_D was applied, the VBM shifts above the conduction band minimum (CBM) of MoS_2, as illustrated in the right panel of Figure 2b. Electrons in the valence band of BP can now tunnel to the conduction band of MoS_2 due to BTBT. As V_D increased, the energy level overlap between the valence band of BP and the conduction band of MoS_2 is enlarged. The number of electrons that can tunnel to the conduction band of MoS_2 increases, leading to a higher reverse current. Basically, the tunneling current is limited by the density of states (DOS) of each component and the tunneling probability. The DOS for 2D materials can be assumed to be constant,[34] while the tunneling probability can be expressed approximately as

$$T(E) = \exp\left[-\frac{2W\sqrt{2m^*(qV_D - E)}}{\hbar}\right]$$

where W is the tunneling barrier width, m^* is the effective mass in the perpendicular direction, $qV_d - E$ represents the tunneling barrier height for an electron of energy E, and $\hbar$ is the reduced Planck constant.[35] We can conclude from the equation that the tunneling current is the most sensitive to W because the tunneling probability depends exponentially on the inverse of W. The atomically thin nature of 2D MoS_2 helps to greatly reduce W, and the vertical structure of the heterojunction expands the contact area of the two components. Both components contribute to the high tunneling current in our device. As the BP thickness is increased further, the higher doping concentration of BP flakes leads to band alignment as shown in Figure 2c. Tunneling takes place at a small reverse V_D, so the reverse current starts to increase at a small reverse V_D as well, which is consistent with the I_D−V_D curve of a backward rectifying diode observed in Figure 1e.

We obtained diverse functional devices including forward rectifying p−n diodes, Zener diodes, and backward rectifying diodes from BP−MoS_2 heterojunctions by varying the BP thickness. No extra doping or gating was included. The device quality can therefore be ensured, and the device can be operated in an energy-efficient manner. Diverse functional diodes can also be achieved through back gate modulation. We fabricated a BP−MoS_2 heterojunction device composed of 44 nm thick BP, from which we obtained the output curves of the junction under various gate biases. A crossover of the output curves in the reverse direction was observed as shown in Figure 3a. Before the crossover gate bias, the current in the reverse direction keeps increasing, and no trend toward saturation was observed. Moreover, the reverse current is orders of magnitude higher than the forward current under high negative gate biases, showing backward rectifying properties. At some point, the reverse current starts to saturate at high reverse V_D, and the current level under forward bias becomes higher than that under reverse V_D, which displays the properties of a forward rectifying p−n diode.

We plotted the output curves of this device in a linear scale under some typical gate biases (−60 V, 10 V, 60 V) in Supporting Information Figure S4. A transition from a backward rectifying diode to a Zener diode and then to a forward rectifying p−n diode can be clearly observed. We then sketched the evolution of forward and reverse current with

DOI: 10.1021/acsnano.7b03994
ACS Nano XXXX, XXX, XXX−XXX

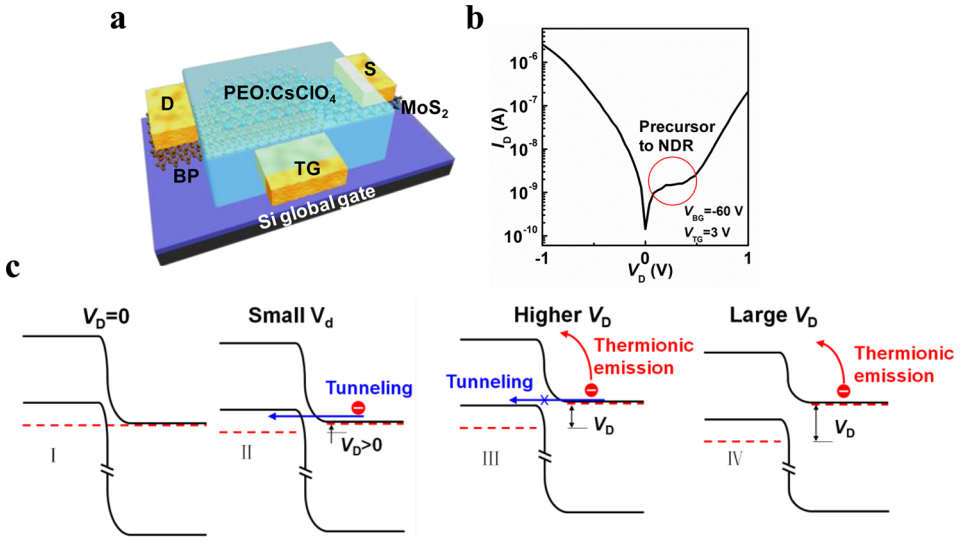

Figure 4. Negative differential resistance. (a) Schematic of a BP−MoS_2 tunnel device with PEO:$CsClO_4$ on the surface. A side gate is patterned on SiO_2 along with the source and drain electrodes. (b) Output curve of a BP−MoS_2 tunnel diode with a precursor toward NDR at V_{BG} = −60 V and V_{TG} = 3 V. (c) Band diagrams explaining the NDR trend.

respect to gate bias in the inset of Figure 3b. As shown, the reverse current at −2 V increased linearly as the negative gate bias decreased, reached a maximum value at around 0 V gate bias, and then decreased. The forward current kept increasing with increasing gate bias. The corresponding rectification ratio was calculated as $I_{2\ V}/I_{-2\ V}$ and is plotted in Figure 3b; as shown, it increases monotonically from 6×10^{-3} to 82. We divided the graph according to the rectification ratio into two regions, i.e., backward and forward rectifying regions. Transfer curves of this BP−MoS_2 heterojunction under V_D = −0.5 V are shown in Figure 3c with some hysteresis. The device was switched on rapidly within a very small gate bias range, and the current was saturated at high gate biases. The transition from the turn-on point to the saturation region was not smooth. This behavior was observed for both forward and reverse sweeps of the transfer curve. The switching and saturation regions correspond to tunneling in the backward rectifying diode and minority carrier drift in the forward rectifying diode, respectively. The diverse device functions achieved through single back gate modulation were attributed to the advantages of using 2D semiconductors. Specifically, carrier concentrations of 2D semiconductors can be effectively modulated by electrostatic gating to produce different functional devices, whereas conventional semiconductors with certain doping concentrations can only lead to devices with a single function. To compare our diverse functional BP−MoS_2 device to a conventional BP−MoS_2 p−n junction device, we fabricated a BP−MoS_2 p−n junction device, and its performance is shown in Supporting Information Figure S5. As shown, a forward rectifying diode behavior was observed despite the back gate modulation. The rectification ratio of the p−n junction device was higher than 1 for all the applied gate biases.

We observed tunneling phenomena in BP−MoS_2 heterojunctions. However, tunneling phenomena originating from a backward rectifying diode or a Zener diode are only incipient, and no NDR region was observed. The NDR effect usually takes place in a tunnel diode with an ultrahigh doping level in the semiconductor components, and it is widely used to make electronic oscillators.[36] Our results have shown great differences in the doping levels of BP flake with different thicknesses. We expected to obtain a higher doping level in the BP by increasing the flake thickness. So, we fabricated a BP−MoS_2 junction device with a BP thickness of 72 nm. Flake thickness was confirmed by AFM in Supporting Information Figure S6, and the optical microscope image is shown beside it. In order to get a higher electron doping concentration in the MoS_2 component, we considered using a top gate for the electrostatic modulation of MoS_2. This is also necessary for obtaining a small SS of the BP−MoS_2 TFET. Under a top gate configuration with a thin high-*k* dielectric, tunneling can be turned on with a much smaller gate bias, and thus a subthermionic SS < 60 mV/dec can be possibly achieved. However, the deposition of conventional high-*k* dielectrics such as Al_2O_3 and HfO_2 on 2D TMDCs (including MoS_2) is still under development, and it is challenging to find the optimized deposition conditions due to the lack of dangling bonds at the TMDCs surfaces.[37]

PEO:$CsClO_4$ solid polymer electrolytes have been applied to TMDCs recently to form a high gate capacitance to explore some potential device properties. A high gate capacitance is formed due to the electric double layer of PEO:$CsClO_4$.[38] Here, we adopted PEO:$CsClO_4$ as a gate dielectric to fabricate a top gate for our BP−MoS_2 heterojunction devices. The synthesis and operation of PEO:$CsClO_4$ is described in detail in the Methods section. We patterned a side gate for the device as shown by the device schematic in Figure 4a. The side gate was deposited together with source and drain electrodes on a SiO_2 substrate.

We then applied dual gating to the device. V_{BG} = −60 V and V_{TG} = 3 V were applied to the back and top gates, respectively. Although there is strong coupling between the back and top gates, the metallic BP screened the electric field from the back gate, and thus the top gate worked more efficiently to the Fermi level modulation of the above MoS_2. n-Type MoS_2 with high electron concentration can be achieved under this gate bias. As a result, a precursor toward NDR was observed in Figure 4b. However, the NDR effect is less pronounced than other reports using different 2D materials. The suppressed NDR trend under a forward bias can be explained by the band diagrams shown in Figure 4c. Since BP is highly p-doped, the Fermi level of BP lies

DOI: 10.1021/acsnano.7b03994
ACS Nano XXXX, XXX, XXX−XXX

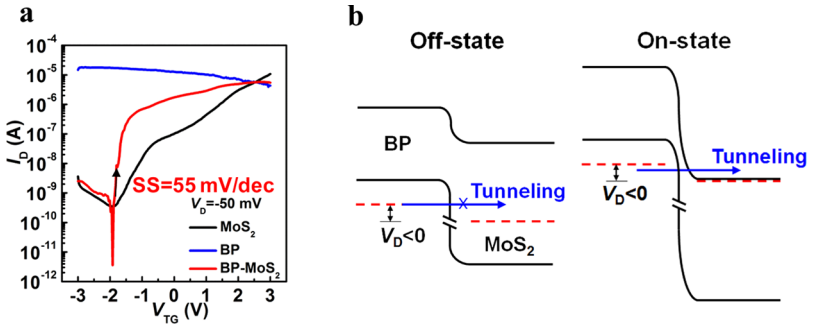

Figure 5. BP−MoS_2 tunneling field effect transistor. (a) Transfer characteristics of BP, MoS_2, and the BP−MoS_2 junction, respectively, under top gate modulation with a PEO:$CsClO_4$ dielectric. (b) Band diagrams explaining the transition of the device from off-state to on-state under top gate modulation.

below the VBM. The CBM of MoS_2 is located slightly below the VBM of BP after band alignment, as shown in part I of Figure 4c, which illustrates the equilibrium state of the BP−MoS_2 junction. When a small forward bias is applied, electrons in the conduction band of MoS_2 immediately tunnel to the valence band of BP as shown in part II of Figure 4c. When we further increased the forward drain bias, the conduction band of MoS_2 aligned with the band gap of BP, and no tunneling current was generated. This situation is shown in part III. Usually, a forward current will decrease in this region, and an NDR can be observed. However, in the case of the BP−MoS_2 junction, thermally emitted electrons over the interface barrier[39] contributed to the electric conduction due to the low interface barrier height formed by the small band gap of BP. So, the conduction mechanism switched from tunneling to thermionic emission in this region. The retarded growth trend in the forward current originated from the current level difference between tunneling and thermionic emission. We thus interpret this trend as a precursor to NDR. The interface barrier was further lowered by increasing the forward bias, as shown in part IV. As a result, the forward current increased monotonically.

The transfer characteristics of BP, MoS_2, and BP−MoS_2 heterojunctions under top gate modulation were then measured and plotted in Figure 5a. We observed a very sharp turn-on in the heterojunction device that starts from −2 V, and the on/off ratio of the device exceeds 10^6 (red curve). We calculated the SS of the heterojunction device according to SS = $d(V_{TG})/d(\log I_D)$. A small SS of 55 mV/dec over a current range of 10^{-10} to ~10^{-8} A was obtained. We confirmed that the small SS comes from tunneling between BP and MoS_2, rather than BP or MoS_2 single components since BP showed degenerate transfer characteristics, while the SS of MoS_2 in this heterojunction was obviously larger than 60 mV/dec. Also note that a traditional MOSFET based on thermionic emission can never achieve an SS smaller than 60 mV/dec. So, we concluded that we successfully achieved a TFET with a BP−MoS_2 heterojunction and a subthermionic SS using the heterojunction TFET. Because of the relatively high leakage current of our PEO:$CsClO_4$ polymer, a small SS was obtained only for a small current range from 10^{-10} to ~10^{-8} A. We expect to achieve a lower off-current in the TFET device and a small SS over a larger current range if we can reduce the leakage current.

The operation mechanism of the BP−MoS_2 TFET under top gate modulation is explained in the band diagrams shown in Figure 5b. Generally, top gate modulation works on the top MoS_2 flake to shift its Fermi level. Under a negative gate bias, the Fermi level of MoS_2 is shifted down toward the midgap, as shown in the left panel of Figure 5b. When the BP Fermi level aligns with the band gap of MoS_2, tunneling cannot take place, and thus the device is turned off at this state. When a positive gate bias is applied, the MoS_2 Fermi level dramatically moves up to its conduction band. After band alignment, the MoS_2 conduction band is almost parallel to the Fermi level of BP, as shown in the right panel. Tunneling can be activated by a very small negative drain bias, and the device switches to its on-state. Since the transition of the device from off-state to on-state is controlled by BTBT, subthermionic SS can be achieved.

CONCLUSION

Tunneling phenomena are observed in BP−MoS_2 heterojunctions. The diode property varied from a conventional forward rectifying diode to a Zener diode and finally became a backward rectifying diode with increasing BP thickness. The diverse device functions can also be achieved through back gate modulation. A subthermionic SS of 55 mV/dec was achieved in a BP−MoS_2 tunnel device with a top gate configuration. A pronounced precursor to NDR was observed under a forward bias on BP when a dual gate was applied.

METHODS

Multilayer BP was prepared using the mechanical exfoliation method. The resulting exfoliated BP was positioned on a highly doped p-Si substrate capped with 285 nm thermally oxidized SiO_2. A MoS_2 flake was then exfoliated onto the poly(dimethylsiloxane) surface and stacked on the BP using a transfer technique. All those processes were done in the glovebox to avoid the oxidation of BP. Before we took out the stacked sample, poly(methyl methacrylate) was coated onto the sample for the next patterning and to protect the sample from the atmosphere. After patterning by electron beam lithography, the sample was loaded to a vacuum electron beam evaporator and 5/80 nm thick Cr/Au was deposited onto the heterostructure to form source and drain contacts. All the measurements were done in a vacuum probe station.

PEO:$CsClO_4$: The preparation and deposition of the polymer electrolyte was performed in an argon-filled glovebox, where the concentrations of H_2O and O_2 inside the glovebox were controlled to <0.1 ppm. PEO (molecular weight 95 000 g/mol) and $CsClO_4$ (99.999%) were dissolved in anhydrous acetonitrile with a molar ratio of PEO ether oxygen to Cs of 76:1 to make a 1 wt % solution. The device was coated with a PEO:$CsClO_4$ solution by drop- casting and then annealed on a hot plate at 100 °C for 10 min to drive off the remaining solvent.

DOI: 10.1021/acsnano.7b03994
ACS Nano XXXX, XXX, XXX−XXX

ASSOCIATED CONTENT

Supporting Information

The Supporting Information is available free of charge on the ACS Publications website at DOI: 10.1021/acsnano.7b03994.

Figures showing flake thicknesses measured by atomic force microscope, logarithmic output curves of diverse functional diodes, output curves of BP and MoS_2 transistors, output curves of the junction device under various gate biases, performances of BP−MoS_2 p−n junction, and thickness of BP measured by AFM (PDF)

AUTHOR INFORMATION

Corresponding Author

*E-mail: yoowj@skku.edu.

ORCID

Hua-Min Li: 0000-0001-7093-4835

Jeong Ho Cho: 0000-0002-1030-9920

Won Jong Yoo: 0000-0002-3767-7969

Author Contributions

#X. Liu and D. Qu contributed equally to this work.

Notes

The authors declare no competing financial interest.

ACKNOWLEDGMENTS

This work was supported by the Global Research Laboratory (GRL) Program (2016K1A1A2912707) and the Global Frontier R&D Program (2013M3A6B1078873) at the Center for Hybrid Interface Materials (HIM), funded by the Ministry of Science, ICT & Future Planning via the National Research Foundation of Korea (NRF).

REFERENCES

(1) Sarkar, D.; Xie, X.; Liu, W.; Cao, W.; Kang, J.; Gong, Y.; Kraemer, S.; Ajayan, P. M.; Banerjee, K. A Subthermionic Tunnel Field-Effect Transistor with an Atomically Thin Channel. *Nature* **2015**, *526*, 91−95.

(2) Ionescu, A. M.; Riel, H. Tunnel Field-Effect Transistors as Energy-Efficient Electronic Switches. *Nature* **2011**, *479*, 329−337.

(3) Ford, A. C.; Yeung, C. W.; Chuang, S.; Kim, H. S.; Plis, E.; Krishna, S.; Hu, C.; Javey, A. Ultrathin Body InAs Tunneling Field-Effect Transistors on Si Substrates. *Appl. Phys. Lett.* **2011**, *98*, 113105.

(4) Khatami, Y.; Banerjee, K. Steep Subthreshold Slope *n*-and *p*-Type Tunnel-FET Devices for Low-Power and Energy-Efficient Digital Circuits. *IEEE Trans. Electron Devices* **2009**, *56*, 2752−2761.

(5) Novoselov, K. S.; Mishchenko, A.; Carvalho, A.; Castro Neto, A. H. 2D Materials and van der Waals Heterostructures. *Science* **2016**, *353*, aac9439.

(6) Lee, C. H.; Lee, G. H.; Van Der Zande, A. M.; Chen, W.; Li, Y.; Han, M.; Cui, X.; Arefe, G.; Nuckolls, C.; Heinz, T. F.; Guo, J.; Hone, J.; Kim, P. Atomically Thin *p-n* Junctions with van der Waals Heterointerfaces. *Nat. Nanotechnol.* **2014**, *9*, 676−681.

(7) Li, L.; Yu, Y.; Ye, G. J.; Ge, Q.; Ou, X.; Wu, H.; Feng, D.; Chen, X. H.; Zhang, Y. Black Phosphorus Field-Effect Transistors. *Nat. Nanotechnol.* **2014**, *9*, 372−377.

(8) Radisavljevic, B.; Whitwick, M. B.; Kis, A. Integrated Circuits and Logic Operations Based on Single-Layer MoS_2. *ACS Nano* **2011**, *5*, 9934−9938.

(9) Gong, C.; Zhang, H.; Wang, W.; Colombo, L.; Wallace, R. M.; Cho, K. Band Alignment of Two-Dimensional Transition Metal Dichalcogenides: Application in Tunnel Field Effect Transistors. *Appl. Phys. Lett.* **2013**, *103*, 053513.

(10) Li, H. M.; Lee, D.; Qu, D.; Liu, X.; Ryu, J.; Seabaugh, A.; Yoo, W. J. Ultimate Thin Vertical *p-n* Junction Composed of Two-Dimensional Layered Molybdenum Disulfide. *Nat. Commun.* **2015**, *6*, 6564.

(11) Lee, S. H.; Choi, M. S.; Lee, J.; Ra, C. H.; Liu, X.; Hwang, E.; Choi, J. H.; Zhong, J.; Chen, W.; Yoo, W. J. High Performance Vertical Tunneling Diodes Using Graphene/Hexagonal Boron Nitride/Graphene Hetero-Structure. *Appl. Phys. Lett.* **2014**, *104*, 053103.

(12) Ilatikhameneh, H.; Klimeck, G.; Appenzeller, J.; Rahman, R. Design Rules for High Performance Tunnel Transistors from 2D Materials. *IEEE J. Electron Devices Soc.* **2016**, *4*, 260.

(13) Ameen, T. A.; Ilatikhameneh, H.; Klimeck, G.; Rahman, R. Few-Layer Phosphorene: An Ideal 2D Material for Tunnel Transistors. *Sci. Rep.* **2016**, *6*, 28515.

(14) Li, L.; Engel, M.; Farmer, D. B.; Han, S. J.; Wong, H. S. High-Performance *p*-Type Black Phosphorus Transistor with Scandium Contact. *ACS Nano* **2016**, *10*, 4672−4677.

(15) Du, Y.; Liu, H.; Deng, Y.; Ye, P. D. Device Perspective for Black Phosphorus Field-Effect Transistors: Contact Resistance, Ambipolar Behavior, and Scaling. *ACS Nano* **2014**, *8*, 10035−10042.

(16) Liu, H.; Neal, A. T.; Zhu, Z.; Luo, Z.; Xu, X.; Tománek, D.; Ye, P. D. Phosphorene: An Unexplored 2D Semiconductor with a High Hole Mobility. *ACS Nano* **2014**, *8*, 4033−4041.

(17) Perello, D. J.; Chae, S. H.; Song, S.; Lee, Y. H. High-Performance *n*-Type Black Phosphorus Transistors with Type Control *via* Thickness and Contact-Metal Engineering. *Nat. Commun.* **2015**, *6*, 7809.

(18) Xiang, D.; Han, C.; Wu, J.; Zhong, S.; Liu, Y.; Lin, J.; Zhang, X. A.; Ping Hu, W.; Ozyilmaz, B.; Neto, A. H.; Wee, A. T.; Chen, W. Surface Transfer Doping Induced Effective Modulation on Ambipolar Characteristics of Few-Layer Black Phosphorus. *Nat. Commun.* **2015**, *6*, 6485.

(19) Yue, D.; Lee, D.; Jang, Y. D.; Choi, M. S.; Nam, H. J.; Jung, D. Y.; Yoo, W. J. Passivated Ambipolar Black Phosphorus Transistors. *Nanoscale* **2016**, *8*, 12773−12779.

(20) Lin, Y. F.; Xu, Y.; Wang, S. T.; Li, S. L.; Yamamoto, M.; Aparecido-Ferreira, A.; Li, W.; Sun, H.; Nakaharai, S.; Jian, W. B.; Ueno, K.; Tsukagoshi, K. Ambipolar $MoTe_2$ Transistors and Their Applications in Logic Circuits. *Adv. Mater.* **2014**, *26*, 3263−3269.

(21) Das, S.; Appenzeller, J. WSe_2 Field Effect Transistors with Enhanced Ambipolar Characteristics. *Appl. Phys. Lett.* **2013**, *103*, 103501.

(22) Liu, X.; Qu, D.; Ryu, J.; Ahmed, F.; Yang, Z.; Lee, D.; Yoo, W. J. *P*-Type Polar Transition of Chemically Doped Multilayer MoS_2 Transistor. *Adv. Mater.* **2016**, *28*, 2345−2351.

(23) Verhulst, A. S.; Sorée, B.; Leonelli, D.; Vandenberghe, W. G.; Groeseneken, G. Modeling The Single-Gate, Double-Gate, and Gate-All-Around Tunnel Field-Effect Transistor. *J. Appl. Phys.* **2010**, *107*, 024518.

(24) Seabaugh, A.; Fathipour, S.; Li, W.; Lu, H.; Park, J. H.; Kummel, A. C.; Jena, D.; Fullerton-Shirey, S. K.; Fay, P. Steep Subthreshold Swing Tunnel FETs: GaN/InN/GaN and Transition Metal Dichalcogenide Channels. *IEEE Int. Electron Dev. Meeting (IEDM)* **2015**, *35.6*, 1.

(25) Liu, Y.; Weiss, N. O.; Duan, X.; Cheng, H.-C.; Huang, Y.; Duan, X. Van der Waals Heterostructures and Devices. *Nat. Rev. Mater.* **2016**, *1*, 16042.

(26) Chakraborty, A.; Sarkar, A. Staggered Heterojunctions-Based Nanowire Tunneling Field-Effect Transistors for Analog/Mixed-Signal System-on-Chip Applications. *Nano* **2015**, *10*, 1550027.

(27) Qu, D.; Liu, X.; Ahmed, F.; Lee, D.; Yoo, W. J. Self-Screened High Performance Multi-Layer MoS_2 Transistor Formed by Using a Bottom Graphene Electrode. *Nanoscale* **2015**, *7*, 19273−19281.

(28) Yan, R.; Fathipour, S.; Han, Y.; Song, B.; Xiao, S.; Li, M.; Ma, N.; Protasenko, V.; Muller, D. A.; Jena, D.; Xing, H. G. Esaki Diodes in van der Waals Heterojunctions with Broken-Gap Energy Band Alignment. *Nano Lett.* **2015**, *15*, 5791−5798.

(29) Hong, T.; Chamlagain, B.; Wang, T.; Chuang, H. J.; Zhou, Z.; Xu, Y. Q. Anisotropic Photocurrent Response at Black Phosphorus-MoS_2 *p-n* Heterojunctions. *Nanoscale* **2015**, *7*, 18537−18541.

DOI: 10.1021/acsnano.7b03994
ACS Nano XXXX, XXX, XXX−XXX

(30) Ye, L.; Li, H.; Chen, Z.; Xu, J. Near-Infrared Photodetector Based on MoS_2/Black Phosphorus Heterojunction. *ACS Photonics* **2016**, *3*, 692−699.
(31) Deng, Y.; Luo, Z.; Conrad, N. J.; Liu, H.; Gong, Y.; Najmaei, S.; Ajayan, P. M.; Lou, J.; Xu, X.; Ye, P. D. Black Phosphorus-Monolayer MoS_2 van der waals Heterojunction *p-n* Diode. *ACS Nano* **2014**, *8*, 8292−8299.
(32) Lan, C.; Li, C.; Wang, S.; He, T.; Jiao, T.; Wei, D.; Jing, W.; Li, L.; Liu, Y. Zener Tunneling and Photoresponse of a WS_2/Si van der Waals Heterojunction. *ACS Appl. Mater. Interfaces* **2016**, *8*, 18375−18382.
(33) Choi, M. S.; Qu, D.; Lee, D.; Liu, X.; Watanabe, K.; Taniguchi, T.; Yoo, W. J. Lateral MoS_2 *p-n* Junction Formed by Chemical Doping for Use in High-Performance Optoelectronics. *ACS Nano* **2014**, *8*, 9332−9340.
(34) Brivio, J.; Alexander, D. T.; Kis, A. Ripples and Layers in Ultrathin MoS_2 Membranes. *Nano Lett.* **2011**, *11*, 5148−5153.
(35) Jena, D. Tunneling Transistors Based on Graphene and 2-D Crystals. *Proc. IEEE* **2013**, *101*, 1585−1602.
(36) Wang, L.; Wasige, E. A Design Procedure For Tunnel Diode Microwave Oscillators. *Proc. Int. Conf. Microw. Millim. Wave Technol.* **2008**, *2*, 832−834.
(37) Yang, J.; Kim, S.; Choi, W.; Park, S. H.; Jung, Y.; Cho, M. H.; Kim, H. Improved Growth Behavior of Atomic-Layer-Deposited High-*k* Dielectrics on Multilayer MoS_2 by Oxygen Plasma Pretreatment. *ACS Appl. Mater. Interfaces* **2013**, *5*, 4739−4744.
(38) Xu, H.; Fathipour, S.; Kinder, E. W.; Seabaugh, A. C.; Fullerton-Shirey, S. K. Reconfigurable Ion Gating of 2h-$MoTe_2$ Field-Effect Transistors Using Poly (ethylene oxide)-$CsClO_4$ Solid Polymer Electrolyte. *ACS Nano* **2015**, *9*, 4900−4910.
(39) Roy, T.; Tosun, M.; Cao, X.; Fang, H.; Lien, D.-H.; Zhao, P.; Chen, Y.-Z.; Chueh, Y.-L.; Guo, J.; Javey, A. Dual-Gated MoS_2/WSe_2 van der Waals Tunnel Diodes and Transistors. *ACS Nano* **2015**, *9*, 2071−2079.

DOI: 10.1021/acsnano.7b03994
ACS Nano XXXX, XXX, XXX−XXX